32. Organic Diodes Based on Redox-Polymer Bilayer-Film-Modified Electrodes

by **Wenyuan Zhao**, **Judith Marfurt**, and **Lorenz Walder***

Institut für Organische Chemie, Universität Bern, Freiestr. 3, CH-3012 Bern

(6.VII.93)

The synthesis of four electropolymerizable 2,2′-bipyridinium salts with tuned reduction potential (E_1°) is described (*N,N′*-ethylene-4-methyl-4′-vinyl-2,2′-bipyridinium dibromide (**4**; $E_1^\circ = -0.48$ V), 4-methyl-*N,N′*-(trimethylene)-4′-vinyl-2,2′-bipyridinium dibromide (**5**; $E_1^\circ = -0.66$ V), *N,N′*-ethylene-4-methyl-4′-[2-(1*H*-pyrrol-1-yl)ethyl]-2,2′-bipyridinium bis(hexafluorophosphate) (**6b**; $E_1^\circ = -0.46$ V), and 4-methyl-4′-[2-(1*H*-pyrrol-1-yl)ethyl]-*N,N′*-(trimethylene)-2,2′-bipyridinium bis(hexafluorophosphate) (**7b**; $E_1^\circ = -0.66$ V)). E_1°-Tuning is based on the torsional angle C(3)–C(2)–C(2′)–C(3′), imposed by the *N,N′*-ethylene and *N,N′*-(trimethylene) bridge. The vinylic compounds **4** and **5** undergo cathodic, the pyrrole derivatives **6b** and **7b** anodic electropolymerization on glassy carbon electrodes from MeCN solutions, yielding thin, surface-confined films with surface concentrations of redox-active material in the range $5 \cdot 10^{-9} < \Gamma < 2 \cdot 10^{-8}$ mol/cm^2, depending on experimental conditions. The modified electrodes exhibit reversible 'diquat' electrochemistry in pure solvent/electrolyte. Copolymerization of **6b** or **7b** with pyrrole yields most stable electrodes. Bilayer-film-modified electrodes were prepared by sequential electropolymerization of the monomers. The assembly electrode/poly-**6b**/poly-**7b** behaves as a switch, it transforms – as a *Schmitt* trigger – an analog input signal (the electrode potential) into a digital output signal (redox state of the outer polymer film). Forward-(electrode/poly-**7b**/poly-**6b**) and reverse-biased assemblies (electrode/poly-**6b**/poly-**7b**) were coupled to the electrochemical reduction of redox-active solution species, *e.g. N*-(cyanomethyl)-*N′*-methyl-4,4′-bipyridinium bis(hexafluorophosphate) (**8**). *Zener*-diode-like behavior was observed. Aspects of redox-polymer multilayer-film assemblies, sandwiched between two electronic conductors, are discussed in terms of molecular electronic devices.

1. Introduction. – Unidirectional electron flow within an ordered structure is a fundamental phenomenon, highly exploited in technology and by living organisms. Typical exponents are current rectifying devices (diodes, transistors) [1a], aspects of the respiratory chain [1b], photovoltaic cells [1a], the photosynthetic reaction center [1c], and synthetic, molecular triads with long-lived charge-separated states [1d, e]. The underlying common principle of all these 'diodes' is a *persistent potential or electrochemical gradient seated within the device* and a *distinct direction of that gradient with respect to the structure of the device*. In modern electronics, this is realized by the band-bending in the n-p-junction region of doped semiconductors, in nature, by orientated cascades of redox systems with continuously tuned E°. In both cases, electrons flow through the device according to the gradient, preferentially from one to the other polar terminal. However, there are differencies with respect to the size, to the mechanism of electron flow and its control (gating), and to the philosophy of building up large networks. Classical semiconductor-based diodes rely on the electronic conductivity in band structures, and can be 'wired' and miniaturized down to the sub-micrometer scale, whereas biological diodes are based on nanometer-sized structures with appropriately coupled molecular orbitals, and nature 'wires' them with mobile electron-transfer (e.t.) shuttles or with rigid e.t. paths of 'high

conductivity' (for a recent debate on long-range biological e.t., see [2]). Gating in field-effect transistors is accomplished by an electrode that controls the conductivity of a thin semi-conducting region *via* surface charges, and, in nature, by molecular species, that interfere specifically with a component of the redox cascade. The miniaturization and fabrication of complex electronic networks (integrated circuits) is based on lithographic techniques including irreversible etching processes (top-down approach), to be compared with nature's reversible self-assembling techniques of molecular components, combined with molecular coding and repairing mechanisms (bottom-up approach).

In brief, there exist serious reasons for the *quest for organic molecular electronics* [3]: the size advantage (*ca.* 2 orders of magnitude in length of a redox cascade as compared to a classical p-n junction), the molecular control of current flow (sensor applications), and nature's advanced assembling, wiring, coding, and repairing techniques.

Our present work is related to the more narrow interpretation of molecular electronics, *i.e.* to the search for molecular material-based semiconductor analogs such as diodes, transistors, and switches.

As pointed out twenty years ago by *Aviram* and *Ratner*, the ultimate molecular rectifier is a linear arrangement of a π-electron donor, covalently linked by an electron-tunneling bridge to a π-electron acceptor and in contact with two electronic conductors, *i.e.* a cylindrical structure of 1–2 nm length and *ca.* 0.5 nm diameter [4]. So far, it is not possible to interface a single molecule of such a size between two conductors [5a]. However, as the diode phenomenon is one-dimensional, there are no restrictions with respect to the remaining two space dimensions, and effectively, monolayers of oriented donor-acceptor molecules, substituted by long alkyl chains and sandwiched between two conducting surfaces by *Langmuir-Blodgett* (*LB*) techniques, were recently shown to exhibit diode current-voltage characteristics, the current on-set voltage being related to the potential difference of the acceptor's electron affinity and the donor's ionization potential [5b–c].

The 'wet' analogs of such assemblies are diodes consisting of two covalently linked redox couples with different $E°$, parallel oriented and sandwiched between two electrodes (*Fig. 1*). According to *Marcus* theory, there exists a parabolic relation between the activation barrier and the driving force for e.t. between $redox_1$ and $redox_2$ [6a, b]. Depending on the sign of the cell voltage and on the orientation of the device, the rate of intramolecular e.t. will be fast, if exergonic – but not yet in the inverted region (forward-biased diode), or slow, if endergonic (reverse-biased diode, *Fig. 1a–c*). Very few covalently linked redox systems, freely diffusing [7a] or immobilized as monolayers on electrode surfaces, were reported to exhibit diode behavior [7b, c]. A more promising technique of preparation of such a diode consists in the electropolymerization of a thin layer of redox couple 1 onto the surface of an electrode, followed by the electropolymerization of another thin layer of redox couple 2, each polymer film corresponding to several theoretical monolayers of the redox couple (for reviews on electropolymerization, chemically modified electrodes, and conducting polymers, see [8]). This architecture prevents short circuits between the two electronic conductors and insures a well-defined, average electrochemical gradient to result at the polymer 1/polymer 2 interface. Provided that the self-exchange e.t. rate between identical redox sites is fast as compared to the endergonic e.t. between redox couple 1 and 2, the diode behavior should not be affected. Such a diode would span a few tenths of nanometer in thickness and could be scaled down to the lithographic limit in the other two space dimensions.

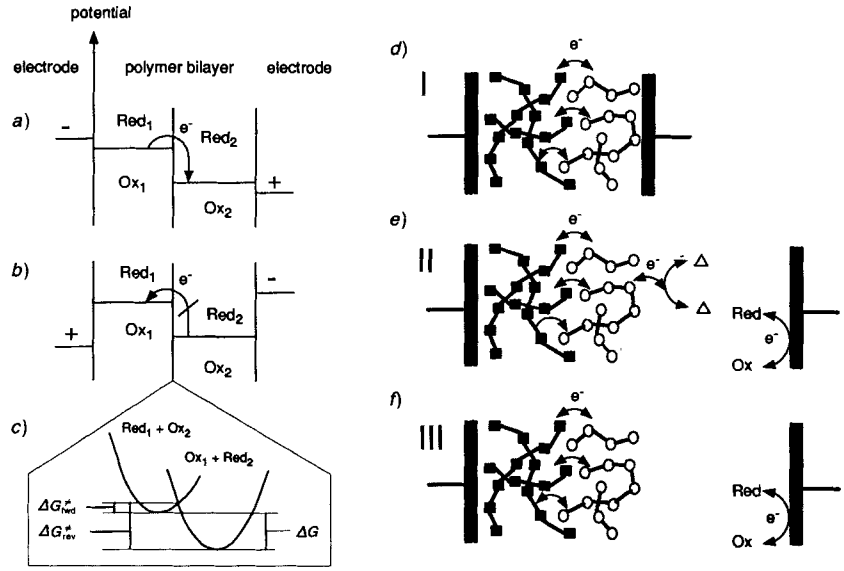

Fig. 1. *Molecular diodes based on redox-polymer bilayer-film-modified electrodes. a)–c)*: Principles; *a)* forward-biased diode, *b)* reverse-biased diode, *c)* free-energy activation barriers at the redox junction represented as *Marcus*-type parabolas. *d)–f)*: Schematic construction, filled squares = $redox_1$, open circles = $redox_2$; *d)* bilayer sandwiched between two conductors (type I); *e)* bilayer coupled to a homogeneous redox species (triangle; type II); *f)* bilayer, ideally polarized at the polymer/solution interface (type III).

Murray and coworkers were the first to realize redox-polymer bilayer-film-modified electrodes, using two segregated, polymeric, thin films with different redox-active metal complexes [9a]. Since then, a few organic redox systems in combination with metal complexes [9], and, more recently, electronically conducting polymers, *e.g.* doped polypyrrole and polythiophene combinations [10] [11], were shown to exhibit diode properties if polymerized as segregated thin films on electrode surfaces. Three types of bilayer constructions emerged (*Fig. 1d–f*), and their potential use in molecular electronics was discussed [12]:

1) Polymer bilayers sandwiched between two electrodes [13] or side by side constructions of two touching redox polymers grown on two sub-micrometer-spaced conducting lines [14], allowing the direct measurement of current-voltage characteristics (*Fig. 1d*, type I).

2) Bilayer assemblies in contact with a single electrode surface and coupled on the solution side to a homogeneous redox system [9d,e] (*Fig. 1e*, type II), *i.e.* only the potential at the polymer/electrode interface can be adjusted *via* the cell voltage, and the complete current-voltage characteristics have to be constructed from measurements with different solution redox species and from both possible arrangements of the outer and inner polymer.

3) Bilayer-modified electrodes which are not coupled to a solution redox species, *i.e.* no steady-state currents can be drawn, but so-called charge-trapping phenomena in the outer redox-polymer film may be observed [9a–d] (*Fig. 1f*, type III).

Strictly speaking, only type-I constructions can be called diodes. However, the phenomena observed with type-II and -III assemblies can easily be extrapolated to the

expected behavior of the corresponding sandwich constructions, and in this paper, the notion 'diode' is used whenever these phenomena occur[1]). We report on purely organic-material-based diodes with open-face architecture, such as of types II and III in *Fig. 1*. For this purpose, we synthesized new electropolymerizable diquat homologues with sterically tuned reduction potentials. Diode phenomena were achieved for the first time with polymer 1/polymer 2 interfacial potential differences as low as 200 mV. In terms of electronic devices, our bilayers behave as organic analogs of *Zener* diodes and 'bistable multivibrators' (*Schmitt* triggers).

2. Retrosynthesis of a Diode. Steric Tuning of Redox Potentials. – A well established synthetic approach to open-face, redox-polymer bilayer-film-based diodes (*cf. Chapt. 1*) is shown in *Scheme 1* [9–11]. It consists of the sequential electropolymerization of two redox-active monomers with different $E°$. This technique ensures control of the film thicknesses (from a few theoretical monolayers up to several hundred nm thick films), and it can be used with macroscopic electrodes as well as with nano-structured conducting lines. An *N*-substituted polypyrrole or a styrene-type polymer (not shown in *Scheme 1*) were considered as ideal polymer backbones to hold the redox centers covalently. The

Scheme 1. *Retrosynthesis of a Diode*

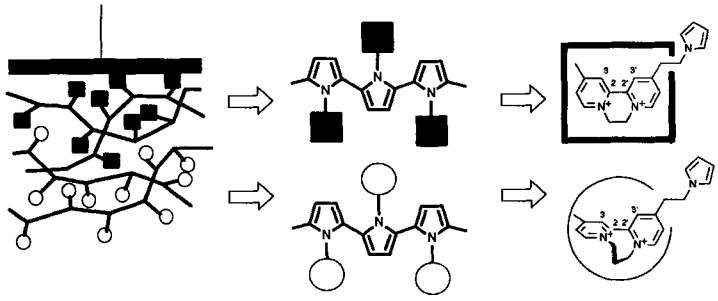

corresponding monomeric pyrrole (or vinyl) derivatives are expected to undergo anodic (cathodic) electropolymerization upon oxidation of the pyrrole subunits (reduction of the vinyl subunits). At such electrode potentials, the surface-confined growing polypyrrole chains are doped (partially oxidized) and exhibit electronic conductivity, ensuring charge-consuming growth at the 'growing polymer'/'solution of monomer' interface. (In case of the polyvinyl chains with appended redox centers, current flow through the polymer and polymerization at the polymer/solution interface relies on an electron-hopping mechanism between the redox centers.) As polymer-bound redox centers we chose diquat (= 1,1′-ethylene-2,2′-bipyridinium = 6,7-dihydrodipyrido[1,2-*a*:2′,1′-*c*]pyrazinediium; *N*,*N*′-ethylene-bridged) and its *N*,*N*′-(trimethylene)-bridged homologue, known to be reduced at *ca.* 0.2 V more negative potentials. Diquat, as other bipyridinium salts,

[1]) Open-face bilayer-film constructions can theoretically be coated with conducting material, but this requires specialized experimental techniques, and we encountered difficulties with this step. On the other hand, such assemblies have an ideal architecture for sensing molecular guests in the contacting solvent *via* guest-host interaction with redox centers in the outer layer. The charge-trapping or -untrapping phenomenon can then be used to amplify the chemical signal [7b–d].

exhibit generally two monoelectronic reductions, reasonable chemical stability, and fast e.t. kinetics [15]. The first reduction potential in the 2,2′-bipyridinium salts is mainly governed by appropriate substituents at C(3), (C(3′)) and N(N′), *i.e.* by those substituent, which determine the torsional angle Θ(C(3)–C(2)–C(2′)–C(3′)) between the planes of the two aromatic rings (*Scheme 1*; for reviews on conformationally controlled reduction potentials, see [16] [17]). The larger Θ, the more negative is E_1°[2]).

3. Synthesis of the Monomers. – Various syntheses of pyrrole-linked 2,2′-bipyridines used as electropolymerizable, bidentate ligands for transition-metal ions were reported in recent years by *Moutet* and *Cosnier* [19]. The main interest was focused on the photoelectrochemical or electrocatalytic properties of the corresponding modified electrodes. Except for the *N,N′*-diquarternization step, we could generally follow their procedures.

Thus, 4-methyl-4′-vinyl-2,2′-bipyridine (**2**) was synthesized from commercially available 4,4′-dimethyl-2,2′-bipyridine *via* the monomethyl ether **1** followed by *t*-BuOK-induced elimination of MeOH from **1** according to the procedure reported by *Abruña et al.*, but modified by a purification step [20] (*cf. Exper. Part*). The corresponding pyrrolyl derivative **3** was earlier described by *Cosnier et al.* [19a]. The detailed synthetic procedure is now included in the *Exper. Part*. The synthesis of **3** follows the well known Na-catalyzed addition of 1*H*-pyrrole to 4-vinylpyridine [21]. The vinyl-diquat **4** (earlier described by *Willman* and *Murray* [9c]) as well as the new homologue **5** are both available from **2** by ring-forming alkylation using 1,2-dibromoethane and 1,3-dibromopropane as a solvent, respectively (*cf. Exper. Part*). The same strategy was also applied to the syntheses of the two new, electropolymerizable, pyrrolyl-substituted 2,2′-bipyridinium dibromides **6a** and **7a** from **3** (*cf. Exper. Part*). In case of **6a**, the ring-forming *N,N′*-alkylation was also performed under high pressure (5.5 kbar instead of normal pressure), but lower reaction temperature (50° instead of 100°). As judged from spectral data, these milder conditions yielded bipyridinium salts of similar quality, but, astonishingly, the high-pressure product did electropolymerize better. To circumvent Br_2 evolution during the intended oxidative polymerization of the pyrrolyl subunits, the corresponding PF_6^- salts **6b** and **7b** were prepared. Both crystallized as charge-transfer complexes with 1 equiv. of NH_3, as indicated by the elemental analyses (*cf. Exper. Part*). The viologen derivative **8** was synthesized by sequential alkylation of 4,4′-bipyridine with MeI according to [9c] and chloroacetonitrile followed by counter-ion exchange with NH_4PF_6 (*cf. Exper. Part*). In the course of these studies, **8** was used as a homogeneous redox system with remarkably positive reduction potential related to the electron-withdrawing influence of the CN group (*cf. Table*). Structure elucidation is based on ^{1}H-NMR, ^{13}C-NMR, elemental analysis, UV/VIS, IR, and cyclic voltammetry.

4. Formation of Redox-Polymer Monolayer-Film-Modified Electrodes. – All monomers **4**–**7** contain two types of reversible redox systems, *i.e.* the *N,N′*-ethylene- or *N,N′*-(trimethylene)-bridged 2,2′-bipyridinium subunit, and two types of electropolymerizable subunits, *i.e.* an activated vinyl [22] or an *N*-substituted pyrrolyl group [23][3]). As ex-

---

[2]) In a series of substituted 2,2′-bipyridinium salts, E_1° covers −0.37 to −0.98 V (*vs.* SCE) and correlates linearly with the torsional angle of the dications in the range of 22–91° as modeled by MMX molecular mechanics [17a] and supported by MO calculations on the bipyridinium salts and the corresponding cation radicals as a function of the torsional angle [18].

[3]) For other polymer-matrix surface-confined viologens and diquats, see [9b, c] [24].

Table. *Reduction Potentials* (E_1° and E_2°) *of the Monomers and Corresponding Polymers*[a])

	Monomers		Polymers			
	E_1°	E_2°	E_1°		E_2°	
4	–0.48 (–0.58)[b])	–0.93 (–1.00)[b])	–0.47		–0.91	
5	–0.66 (–0.80)[b])	–0.96 (–1.06)[b])	–0.66	(–0.80)[b])	–0.95	(–1.08)[b])
6b	–0.46 (–0.38)[c])	–0.91 (–0.85)[c])	–0.42[d])	(–0.33)[c])	–0.84[d])	(–0.82)[c])
7b	–0.66 (–0.60)[c])	–0.94 (–0.92)[c])	–0.64[e])	(–0.58)[c])	0.90[e])	(–0.90)[c])
8	–0.27	–0.65				

[a]) In [V] *vs.* SCE, determined by cyclic voltammetry $((E_p(\text{cat.}) + E_p(\text{anod.}))/2$ at $\upsilon = 0.1$ V/s; in 0.1M $Bu_4N(ClO_4)$/MeCN, unless otherwise specified. [b]) In 0.1M $Bu_4N(PF_6)$/MeCN. [c]) In 0.1M $LiClO_4/H_2O$. [d]) Identical with $\mathbf{D_2}$. [e]) Identical with $\mathbf{D_3}$.

pected, the monomers exhibit two well defined reversible redox couples in cyclic voltammetry in the potential range from –0.4 and –1 V *vs.* SCE in 0.1M $Bu_4N(ClO_4)$/MeCN corresponding to the transitions of the dication to the monocation (++ + e^- ⇄ +·; E_1°) and of the monocation to the neutral species (+· + e^- ⇄ °; E_2°; *Table*) [15] [16]. No heterogeneous e.t. kinetics are detectable for scan rates up to 1 V/s. The first reduction potential (E_1°) of **5** and **7** is shifted negatively by 180 and 200 mV as compared to E_1° of **4** and **6**, respectively. This is the envisaged effect of one additional methylene group in the *N*,*N*′-bridge of 2,2′-bipyridinium salts on E_1°, related to an increase of the torsional angle Θ (*Scheme 2*)[2]).

Scheme 2

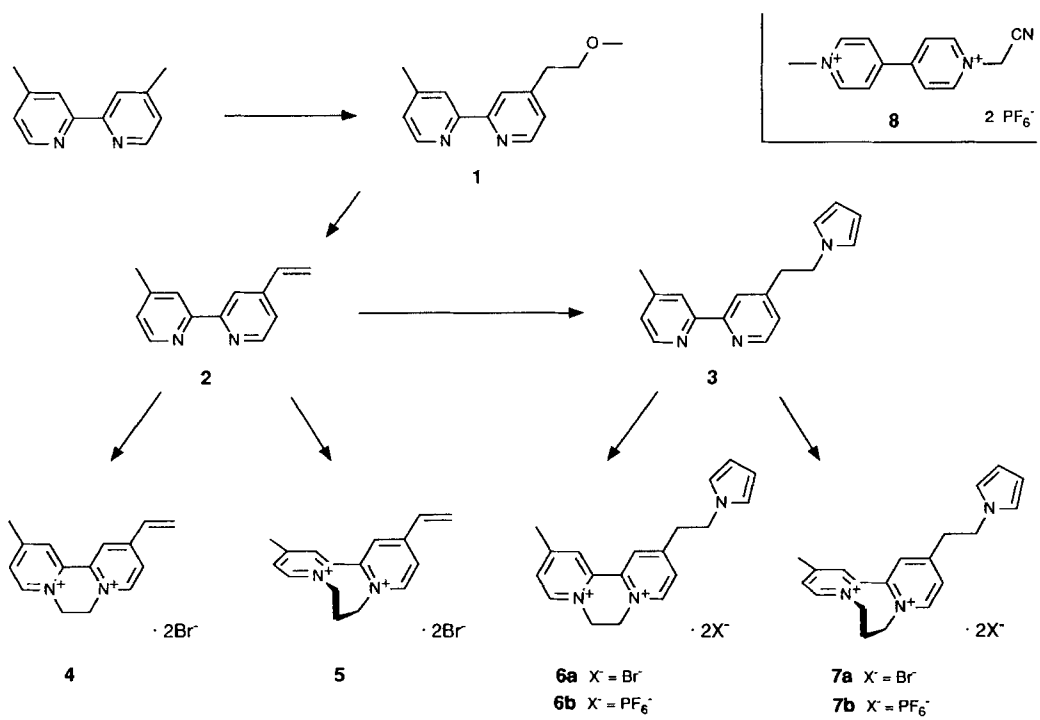

The vinyl-substituted bipyridinium salts **4** and **5** undergo electropolymerization on glassy carbon electrodes from solutions of $Bu_4N(ClO_4)$ or $Bu_4N(PF_6)$/MeCN, if the electrode potential is continuously scanned between 0 and −1.2 V over the two redox couples for 10–100 min or hold at a fixed potential on the negative side of the second redox couple (*cf. Exper. Part*), as anticipated [9c] [22]. If the cycling-potential technique is used, the growth of the surface-confined redox polymer can be monitored from the steadily increasing peak currents (*Fig. 2*). Principally, the cathodic polymerization of activated vinyl compounds is a non-charge-consuming process, and a catalytic amount of electrons may trigger polymerization. However, from our experiments, we conclude that this reaction is not really catalytic in electrons. Polymer growth on the electrode surface requires a cathodic current for the whole period of polymerization. It is mainly based on e.t. between vinylic, dicationic bipyridinium solution species and doubly reduced bipyridinium moieties in the polymer; charge propagation within the polymer occurs by an electron-hopping mechanism. Polymer growth is much slower, if the negative potential limit is restricted to values between E_1° and E_2°. Addition of H_2O speeds up the observed polymerization rate, and **5** electropolymerizes even from pure 0.1M $LiClO_4/H_2O$ (possibly

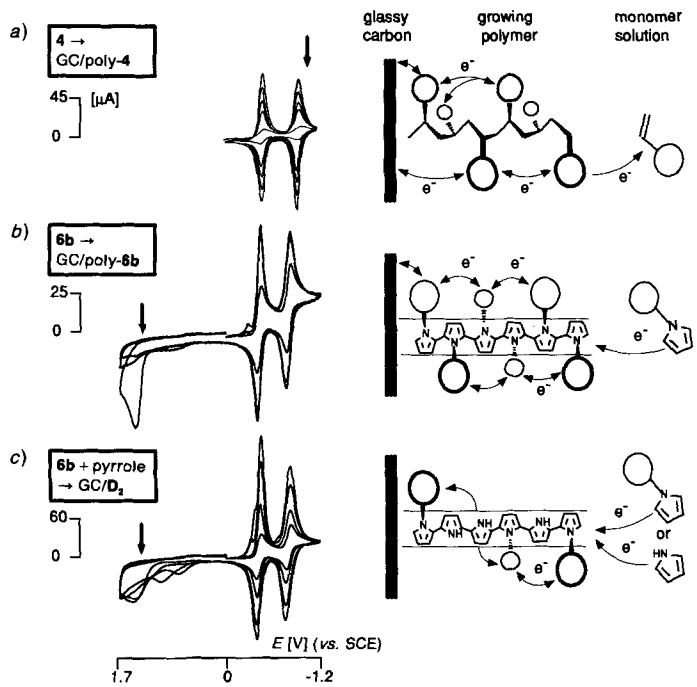

Fig. 2. *Electropolymerization of* **4**, **6b**, *and* **6b**/*pyrrole by repetitive potential cycling* ($v = 0.1$ V/s) *and structural models for the growing polymer chains.* Growth of the electrode-confined polymer is monitored from the increasing peak currents (note: different current scales). *a*) **4** ($1.2 \cdot 10^{-3}$ M) in 0.1M $Bu_4N(ClO_4)$/MeCN + 10% H_2O: scans 1, 3, 8, 15, and 28 displayed, yielding GC/poly-**4**; *b*) **6b** ($1.4 \cdot 10^{-3}$ M) in 0.2M $Bu_4N(ClO_4)$/MeCN: scans 1, 2, and 4 displayed, yielding GC/poly-**6b**; *c*) **6b** ($1.4 \cdot 10^{-3}$ M) + pyrrole ($0.15 \cdot 10^{-3}$ M) in 0.2M $Bu_4N(ClO_4)$/MeCN: scans 1, 2, 4, and 6 displayed, yielding GC/$\mathbf{D_2}$. Bold arrows: potential used for electropolymerization at fixed potentials. Electrode: glassy carbon (= GC; $A = 0.07$ cm^2).

from an adsorbed state). However, such H_2O-grown polymer films are less persistent, and the redox response of poly-**5** tends to break down toward the end of electropolymerization. We did not analyze the structure and molecular weight of poly-**4** and poly-**5**, but we propose a helical alkane chain with the polar substituents pointing outwards for sterical and solubility reasons (*cf.* proposed structure of poly-**4** in *Fig. 2a*).

In addition to their bipyridinium-localized redox activity, the PF_6^- salts **6b** and **7b** exhibit an anodic wave due to the irreversible oxidation of the pyrrolyl group, which undergoes then polymerization [23] (in the corresponding bromides **6a** and **7a**, the wave is covered by Br^- oxidation). The salts **6b** and **7b** are oxidatively electropolymerized from $Bu_4N(ClO_4)$/MeCN, using a repetitive potential scan between 0 and +1.7 V or imposing a fixed potential at the foot of the pyrrole oxidation (*cf. Exper. Part*). In this potential range, the polypyrrole backbone is also oxidized and becomes electronically conductive, *i.e.* the electrode potential is active at the polymer/solution interface and thus guarantees further chain growth, even for thick polymer films. Notably, anodic pyrrole electropolymerization – in contrast to the polymerization of the vinyl salts **4** and **5** – is formally a charge-consuming process coupled to the liberation of two protons. The structure of poly-**6b** and poly-**7b** was not analyzed, but it is supposed to consist mainly of linear chains (or ribbons, because of charge delocalization) of 2,5-linked pyrrole subunits (*cf.* structural model for poly-**6b** in *Fig. 2b*) [23]. Generally, **6b** and **7b** polymerize faster than **4** and **5**, and – with respect to the redox subunit – the ethylene-bridged **6b** polymerizes more efficiently than the trimethylene-bridged **7b**. The latter fact may be related to peripheral steric strain that builds up in the growing polymer chain mainly with the more twisted and, therefore, sterically more demanding redox subunit. To reduce such strain, **6b** and **7b** are coelectropolymerized with unsubstituted pyrrole to give the modified electrodes denoted GC/$\mathbf{D_2}$ and GC/$\mathbf{D_3}$, respectively (*Fig. 2c*, GC = glassy carbon electrode; *cf. Exper. Part*). Such co-electropolymerization yields higher surface concentrations (Γ's) in electroactive bipyridinium for a given polymerization time, in spite that the 'on-chain-density' of bipyridinium subunits is lower[4]). From a crude coulometric analysis, we judge the ratio pyrrole/**6b** *ca.* 1:2 and pyrrole/**7b** *ca.* 1:3, incorporated in $\mathbf{D_2}$ and $\mathbf{D_3}$ (*cf. Exper. Part* and proposed structure for $\mathbf{D_2}$ in *Fig. 2c*) [26]. These are optimized polymer compositions with respect to high stability, large redox currents from the bipyridinium subunits, and acceptable charge-propagation kinetics. They are obtained from monomer concentrations ratios [pyrrole]/[**6b**] = [pyrrole]/[**7b**] $\approx$ 0.2.

The polymer-modified electrodes are checked for their redox activity in monomer-free $Bu_4N(ClO_4)$/MeCN under Ar. Typical responses for surface-confined diquats are observed for all redox polymers, *i.e.* E°'s close to those of the monomers (*Table*), linear *i vs.* *v* correlations up to *ca.* 1 V/s (*Fig. 3c*), an apparent Γ, independent on *v* for $v < 1$ V/s (*Fig. 3d*), and small cathodic-anodic peak separations on the ++/+· wave for $v < 1$ V/s (*Fig. 3e*). The redox responses are reasonably stable under repetitive cyclic voltammetry conditions, but definitely more persistent for $\mathbf{D_2}$ and $\mathbf{D_3}$ as compared to poly-**6b** and poly-**7b**. For a continuous scan between +1 and −1.4 V, 17 and 44% loss of electroactivity for poly-**6b** and poly-**7b**, respectively, and 11 and 9% loss for $\mathbf{D_2}$ and $\mathbf{D_3}$ are observed after 20 min. Definitely less stable responses are obtained with poly-**4** and poly-**5**. All

[4]) A ferrocenyl-pyrrole derivative undergoes electropolymerization only in presence of free pyrrole [25].

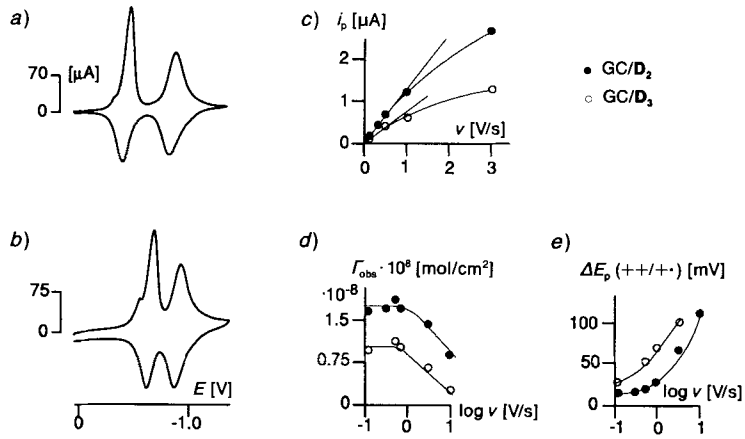

Fig. 3. *Cyclic voltammetry of redox-polymer monolayer-film-modified electrodes.* *a*) GC/$\mathbf{D_2}$ ($\Gamma = 2.1 \cdot 10^{-8}$ mol/cm^2), $v = 100$ mV/s; *b*) GC/$\mathbf{D_3}$ ($\Gamma = 2.4 \cdot 10^{-8}$ mol/cm^2), $v = 100$ mV/s; *c*) representative plots of i_p(++/+·) *vs.* v; *d*) $\Gamma_{obs.}$ (++/+·) *vs.* log v; *e*) ΔE_p (++/+·) *vs.* log v. All measurements in 0.2M $Bu_4N(ClO_4)$/MeCN.

following experiments were, therefore, performed with the most stable $\mathbf{D_2}$ and $\mathbf{D_3}$ polymers.

Using solutions of **6b** or **7b** ($c = 1.4 \cdot 10^{-3}$M) in presence of pyrrole ($c = 0.15 \cdot 10^{-3}$M; *cf. Exper. Part*), a linear correlation of the coulometrically observed diquat surface concentration on the modified electrodes is found in pure solvent/electrolyte from $3 \cdot 10^{-9}$ to $2 \cdot 10^{-8}$ mol/cm^2 with polymerization times from 10 to 180 s. According to a crude estimate, this surface-concentration range corresponds to a film-thickness range of *ca.* 10–80 nm (*cf. Exper. Part*). For all pyrrolyl-based polymers (poly-**6b**, poly-**7b**, $\mathbf{D_2}$, and $\mathbf{D_3}$), a prewave and excess charge in the first reduction wave is observed, due to the reduction of residual oxidized pyrrole sites in the polymer backbone (*Figs. 2* and *3*), but only if the potential is swept in the previous scan into the region of polypyrrole oxidation.

5. The Monolayer Films under Stationary Current Load. Polymer-Mediated Reduction of V_{CN}^{++} in Solution. – A solution of the 4,4′-bipyridinium salt **8** (= V_{CN}^{++}; ($c = 1 \cdot 10^{-3}$M)) in 0.2M $Bu_4N(ClO_4)$/MeCN exhibits two reversible reduction waves with $E_1^\circ = -0.27$ V and $E_2^\circ = -0.65$ V (*vs.* SCE) at a 'naked' rotated glassy carbon electrode (*Fig. 4*). If either a $\mathbf{D_2}$-polymer or a $\mathbf{D_3}$-polymer monolayer-film-modified electrode is used, the reduction wave at −0.27 V is completely suppressed. V_{CN}^{++} does not diffuse through these polymers (gives no permeation reduction current at −0.27 V), probably because of unfavorable electrostatic interaction of the dication with the positively charged polyelectrolyte $\mathbf{D_2}$ and $\mathbf{D_3}$[5]). The current responses due to the polymer-mediated reduction of V_{CN}^{++} are observed in a potential range where the first redox level starts to become populated[6]). As V_{CN}^{++} is more

[5]) Neutral, medium-sized electroactive species such as ferrocene diffuse slowly through the polymer and are detected at the electrode surface.

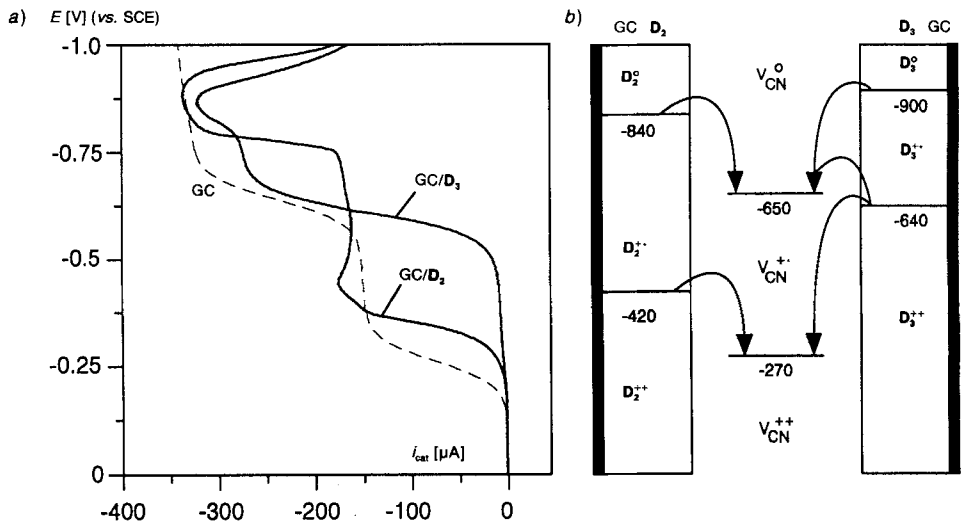

Fig. 4. *Reduction of homogeneous* V^{++}_{CN} (**8**) *mediated by redox-polymer monolayer films. a)* V^{++}_{CN} ($c = 1 \cdot 10^{-3}$ M) in 0.2M $Bu_4N(ClO_4)$/MeCN + pyridine ($50 \cdot 10^{-3}$M) at rotating-disc electrodes ($A = 0.2$ cm^2, $v = 780$ rpm, $v = 5$ mV/s); GC = neat glassy carbon; GC/**D**$_2$ = **D**$_2$-modified glassy carbon ($\Gamma_{6b} = 1.9 \cdot 10^{-8}$ mol/cm^2; preparation: 60 s, 1.29 V); GC/**D**$_3$: **D**$_3$-modified glassy carbon ($\Gamma_{7b} = 1.6 \cdot 10^{-8}$ mol/cm^2; preparation: 75 s, 1.29 V). *b)* Energetics and activation barriers for the mediated reduction of **8**.

easily reduced than $\mathbf{D}_2^{+\cdot}$ and $\mathbf{D}_3^{+\cdot}$ (*cf. Table*), e.t. from both reduced polymers to the V^{++}_{CN} is a thermodynamically favorable process. The limiting plateau current, in case of **D**$_2$-catalysis, is the same as at the naked electrode for the $V^{++}_{CN} \rightarrow V^{+\cdot}_{CN}$ reduction. This picture is not much affected if $[V^{++}_{CN}]$ is increased up to $8 \cdot 10^{-3}$ M, *i.e.* the limiting current grows linearly with $[V^{++}_{CN}]$, as expected, if charge propagation within the polymer is not limiting[7]). At this final concentration, a remarkable current density of 5.5 mA/cm^2 is reached at the **D**$_2$-polymer-modified electrode, however, *ca.* 10% of activity is lost per 1 min under such drastic conditions. The situation is more complicated with the **D**$_3$-modified electrode: As illustrated above, the mediated $V^{++}_{CN} \rightarrow V^{+\cdot}_{CN}$ reduction is thermodynamically favorable and delivers a diffusion-controlled part to the limiting current, but the $\mathbf{D}_3^{+\cdot}/\mathbf{D}_3^{+}$ reduction potential (−0.64 V) coincides with the $V^{+\cdot}_{CN} \rightarrow V^{\circ}_{CN}$ reduction (−0.65 V) and that adds

---

[6]) The potential ($E_{1/2}$) for **D**$_2$- and **D**$_3$-mediated V^{++}_{CN} reduction is shifted positively as compared to E°_1 of **D**$_2$ (*cf.* small current hump in *Fig. 4*) and of **D**$_3$ by 90 and 55 mV, respectively. The catalytic current may be limited by e.t. at the electrode/polymer interface, within the polymer, at the polymer/solution interface, or by diffusion of V^{++}_{CN}. The asymmetry of the polarogram (slow current increase with potential at the foot of the waves and abrupt change of the slope at its top into the limiting current) indicates: limitation by charge transfer in the polymer in the foot and limitation by V^{++}_{CN} diffusion (in case of GC/**D**$_2$) or by charge transfer at the polymer/solute interphase (in case of GC/**D**$_3$) at the top of the wave[7]).

[7]) A more accurate analysis of the limiting currents at a redox-polymer-modified rotated-disc electrode is based on $1/i_l$ *vs.* $1/\omega^{1/2}$ representations (*Koutecky-Levich* plots) [27]. In this work, no variable-rotation-rate (ω) studies were performed.

another part to the total mediated current[8]). If the potential of the $\mathbf{D}_2$- or the $\mathbf{D}_3$-modified electrode is driven to more negative values, the second redox process of the modifiers becomes involved. Now, for both polymers, the first ($V_{CN}^{++} \rightarrow V_{CN}^{+\cdot}$) and second ($V_{CN}^{+\cdot} \rightarrow V_{CN}^{0}$) reduction of the solution species are thermodynamically favorable, and diffusion-limited currents are observed (at least for $[V_{CN}^{++}] \leqslant 2 \cdot 10^{-3}$ M). However, under such conditions, the electrodes loose *ca.* 20% of their activities within 30 s. This irreversible degradation has not been further studied and is not reproducible very well.

6. An Organic *Schmitt*-Trigger: Switching and Charge-Trapping Properties of the Redox-Polymer Bilayer Film. – Electropolymerization from a MeCN solution containing **6b**/**7b**/pyrrole 1:1:0.2 leads to a modified glassy carbon electrode, denoted GC/$\mathbf{D}_2 + \mathbf{D}_3$. Sequential electropolymerization from a solution of **6b** and pyrrole in MeCN followed by another electropolymerization onto the modified electrode, from **7b** and pyrrole in MeCN, affords the redox-polymer bilayer-film-modified electrode GC/$\mathbf{D}_2$/$\mathbf{D}_3$. The reverse procedure is used to prepare GC/$\mathbf{D}_3$/$\mathbf{D}_2$ (*cf. Exper. Part*).

The cyclic voltammogram of GC/$\mathbf{D}_2 + \mathbf{D}_3$ (*Fig. 5a*) in pure solvent-electrolyte corresponds essentially to the overlaid responses of the monolayer-modified electrodes GC/$\mathbf{D}_2$ and GC/$\mathbf{D}_3$ with the second redox couple being not resolved as $E_2^{\circ}(\mathbf{D}_2) - E_2^{\circ}(\mathbf{D}_3) = 60$ mV. A slight preference for the incorporation of **6b** over **7b** into the polymer is consistent with the observations described in *Chapt. 4*. In GC/$\mathbf{D}_2 + \mathbf{D}_3$, there exist four redox levels, which extend from the electrode surface to the polymer/solution interface, and these equilibrate with the electrode potential on the time scale of cyclic voltammetry.

The cyclic voltammogram of GC/$\mathbf{D}_2$/$\mathbf{D}_3$ (*Fig. 5b*) exhibits essentially the inner-layer $\mathbf{D}_2$ response overlaid by two current spikes, which are separated by *ca.* 0.3 V. This phenomenon is related to the architecture of the polymer, consisting of two segregated layers, each with its two proper redox levels. The redox levels of the inner layer equilibrate fast with the electrode potential. However, to populate the redox levels of the outer layer, e.t. in one direction at the polymer/polymer interface involves a large activation barrier (*Fig. 1*). Thus, no redox waves are observed for the outer-layer first redox couple for electrode potentials in the vicinity of $E_1^{\circ}(\mathbf{D}_3)$, but the charge shoots into the outer layer as soon as the second inner redox level starts to become reduced, opening a new mechanism for e.t. at the polymer/polymer interface (spike formation). On the oxidative scan, the outer layer is – for the same reason – not discharged at $E_1^{\circ}(\mathbf{D}_3)$, *i.e.* the charge is trapped in the outer layer, but electrons shoot, if the electrode potential has reached the foot of the first anodic wave (charge untrapping). In terms of electronic devices, *such behavior is typical for a bistable multivibrator or* Schmitt *trigger, able to transform the treshold of an analog signal* (the electrode potential) *into a digital signal* (redox state of the outer polymer). For the inverse sequence of redox polymers (*Fig. 5c*), essentially the inner layer $\mathbf{D}_3$ response without spike formation is obtained. The bilayer properties show up, if a sequential scan $0 \rightarrow -1.4 \rightarrow 0 \rightarrow -1.4 \rightarrow 0$ V is performed: The cathodic peak for the $\mathbf{D}_3^{++}$ reduction drops drastically on the second scan. This is related to the charge that stays trapped in the outer layer as indicated by the activation barriers involved (*Fig. 5c*).

---

[8]) At $[V_{CN}^{++}] = 1 \cdot 10^{-3}$ M, the additional current mediated by $\mathbf{D}_3^{+\cdot}$ is supposed to be charge-transfer-controlled at the polymer/solute interphase as it reaches only *ca.* 80% of i_l at the bare electrode, but does go to 100% at more negative potentials where $\mathbf{D}_3^{\S}$ is involved in catalysis [28].

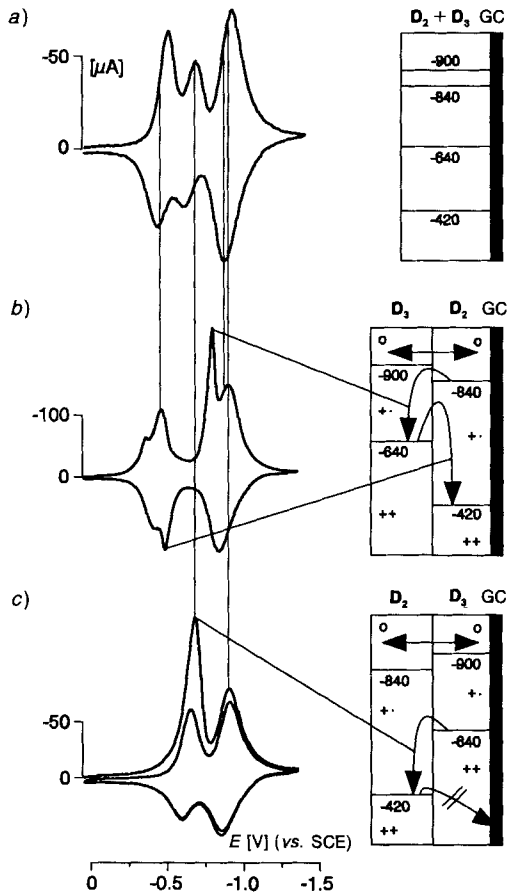

Fig. 5. *Switching and charge-trapping processes at redox-polymer bilayer-film-modified glassy carbon electrodes* ($A = 0.07$ cm^2, Γ in mol/cm^2) *in 0.2* M *$Bu_4N(ClO_4)$/MeCN at* $v = 100$ mV/s. *a*) Copolymer (**6b** + **7b**) monolayer ($\Gamma_{6b} \approx 5 \cdot 10^{-9}$, $\Gamma_{7b} \approx 4 \cdot 10^{-9}$) all redox levels equilibrate. *b*) GC/$\mathbf{D_2}$/$\mathbf{D_3}$ ($\Gamma_{6b} \approx 2.4 \cdot 10^{-8}$, $\Gamma_{7b} \approx 1 \cdot 10^{-8}$), charge in the outer layer is trapped and untrapped. *c*) GC/$\mathbf{D_3}$/$\mathbf{D_2}$ ($\Gamma_{7b} \approx 8 \cdot 10^{-9}$, $\Gamma_{6b} \approx 5 \cdot 10^{-9}$), charge in the outer layer is trapped (see text).

Charge untrapping occurs by chemical oxidation of the outer redox couple or electrochemically, if a very positive electrode potential in the range of polypyrrole oxidation is applied. In the latter case, the polypyrrole backbone becomes electronically conducting and that opens a new mechanism for $\mathbf{D_2^{+\cdot}}$ oxidation.

Spike formation (*Fig. 5b*) is observed for sweep rates (v) $0.01 \leqslant v \leqslant 1$ V/s. With increasing v, the cathodic and the anodic spike drift apart, and for $v > 1$ V/s, they merge with the $\mathbf{D_2^{+\cdot}}$ reduction and the $\mathbf{D_2^{+\cdot}}$ oxidation, respectively. Thus, the redox-polymer bistable multivibrator is orders of magnitude slower than its solid-state counterpart. This drawback is related to the kinetics of charge diffusion through the polymer (electrons and counter ions) involved in the complete reduction or oxidation of the bilayer, *i.e.* similar

limiting kinetics as in case of the cyclic voltammetry of the monolayers are expected (*Fig. 3*). To increase the apparent charge-transfer kinetics, one has to decrease the film thickness and will ultimately end up with *Aviram*'s conception [4], *i.e.* a molecular monolayer of highly ordered, linear molecules with two redox subunits. Notably, charge transport through a mono- or bilayer film (forward-biased) under stationary conditions, *i.e.* coupled to a homogeneous redox couple or in contact with another conductor (*Figs. 1d* and *1e*), may be much faster than expected from measurements done with the film with ideally polarized polymer/solution interface (III in *Fig. 1f*), because under type-I/II conditions, only electrons have to move, whereas under type-III conditions, both electrons and counter ions have to move.

7. An Organic *Zener*-Diode: Mediated V_{CN}^{++} Reduction under Forward and Reverse Bias. – Rotating-disc voltammograms showing the reduction of the solution species V_{CN}^{++} (**8**) at the bare glassy carbon electrode (GC), at the forward-biased bilayer-modified electrode ($GC/D_3/D_2$), and at the reverse-biased bilayer-modified electrode ($GC/D_2/D_3$) are compared in *Fig. 6*. As in the case of monolayer films, only mediated V_{CN}^{++} reduction is expected, but additional kinetic restrictions, related to the directional e.t. at the polymer/polymer interface, are now operative.

In case of the forward-biased polymer assembly ($GC/D_3/D_2$) current starts to flow at −0.5 V and reaches a sharp peak at −0.7 V, *i.e.* in the vicinity of the first available inner-film redox couple ($E°(D_3^{++}/D_3^{+}) = -0.64$ V). The current seems to be again polymer charge-transfer-controlled at the foot of the wave but diffusion-limited at more negative

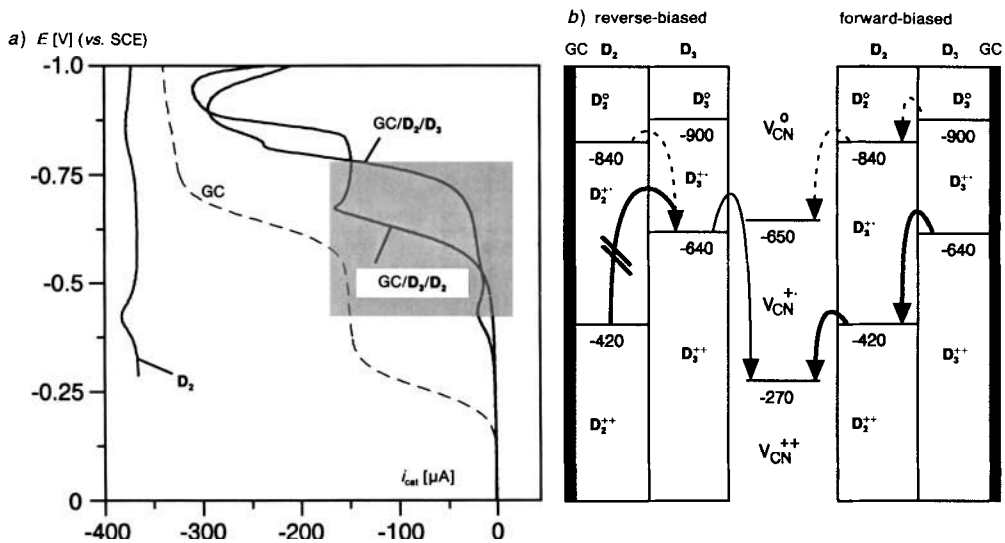

Fig. 6. *Reductions of homogeneous* V_{CN}^{++} (**8**) *mediated by redox-polymer bilayer films. a*) [**8**] = $1 \cdot 10^{-3}$ M in 0.2M $Bu_4N(ClO_4)$/MeCN + pyridine ($50 \cdot 10^{-3}$ M) at rotating-disc electrodes ($A = 0.2\ cm^2$, $v = 780$ rpm, $\nu = 5$ mV/s, Γ in mol/cm^2). GC = neat glassy carbon; $GC/D_3/D_2$ = forward-biased diode ($\Gamma_{7b} \approx 0.8 \cdot 10^{-8}$, $\Gamma_{6b} \approx 0.8 \cdot 10^{-8}$); $GC/D_2/D_3$ = reverse-biased diode ($\Gamma_{6b} \approx 2.1 \cdot 10^{-8}$, $\Gamma_{7b} \approx 1.6 \cdot 10^{-8}$); D_2 = GC/D_2 electrode ($\Gamma_{6b} = 2.1 \cdot 10^{-8}$) without **8** in solution, but otherwise same experimental conditions; grey region: potential range exhibiting diode properties. *b*) Energetics and activation barriers for the bilayer-mediated reduction of **8**.

potentials (the same plateau as observed at the naked electrode is reached). Up to $8 \cdot 10^{-3}$ M, the limiting current follows linearly $[V_{CN}^{++}]$. Thus, the forward-biased GC/$\mathbf{D_3}$/$\mathbf{D_2}$ exhibits voltammograms similar to those of the monolayer-film electrode GC/$\mathbf{D_3}$[9]). In case of the reverse-biased bilayer electrode (GC/$\mathbf{D_2}$/$\mathbf{D_3}$), only a tiny current hump followed by a small plateau current ($i_{l(rev.)} = 25 \pm 5$ mA) is observed, when the electrode potential has moved over the first inner-film redox couple with $i_{l(rev.)}$ being not influenced by $[V_{CN}^{++}]$ for $1 \cdot 10^{-3} < [V_{CN}^{++}] < 8 \cdot 10^{-3}$ M[10]). No additional current is observed, when the first outer-film redox couple $E°(\mathbf{D_3}^{++}/\mathbf{D_3}^{+})$ is reached. These differences, depending on the sequence of the polymers $\mathbf{D_2}$ and $\mathbf{D_3}$ on the electrode, are ascribed to the directional kinetic barrier for e.t. at the polymer/polymer interface. In case of GC/$\mathbf{D_3}$/$\mathbf{D_2}$ (forward-biased diode), e.t. at the $\mathbf{D_3}$/$\mathbf{D_2}$ interface is an exergonic reaction and, therefore, fast and not limiting the current, whereas in case of GC/$\mathbf{D_2}$/$\mathbf{D_3}$ (reverse-biased diole), e.t. at the $\mathbf{D_2}$/$\mathbf{D_3}$ interface is endergonic and thus slow and limiting the current. If – under reverse bias – the electrode potential is moved more negative, the second redox level of the inner film ($E°(\mathbf{D_2}^{+}/\mathbf{D_2}^{0}) = -0.84$ V) becomes populated and opens a new mechanism for fast electron flow through the bilayer assembly. Under these conditions, the current reaches a limiting value, similar to that observed at the $\mathbf{D_2}$ monolayer-film-modified electrode. However, an irreversible and not well reproducible decay of the current response is observed, as in case of the monolayer films. The expected current-voltage characteristics of the hypothetical sandwich construction electrode/$\mathbf{D_2}$/$\mathbf{D_3}$/electrode can be predicted. It should show current under forward bias and current break-through under reverse bias for a given potential treshold as in case of a *Zener* diode [29].

8. Conclusions and Perspectives for 'Wet' Electronic Devices with Redox Junctions. – It is tempting to extrapolate the current-voltage characteristics of open-face redox-polymer assemblies to those of the corresponding structures sandwiched between two conductors. The latter constructions are distinguished for their redox 1/redox 2 interface, *i.e.* a redox junction, as compared to the conventional solid-state devices with a p-n junction. An important aspect of the performance of a diode (type I in *Fig. 1*), is the ratio of the limiting currents under forward ($i_{l(f.b.)}$) and reverse ($i_{l(r.b.)}$) polarization. Ideally, the leakage current ($i_{l(rb.)}$) is related to the endergonic e.t. rate at the redox-polymer-1/redox-polymer-2 interface, *i.e.* at the redox junction, and can be described for the hypothetical diquat diode, electrode/$\mathbf{D_2}$/$\mathbf{D_3}$/electrode, by *Eqn. 1* with

$$i_{l(r.b.)} = n \cdot F \cdot A \cdot k_{(\mathbf{D_2} \rightarrow \mathbf{D3})} \cdot \Phi_1(\mathbf{D_2}^{+}) \cdot \Phi_2(\mathbf{D_3}^{++}) \qquad \text{(reverse bias)} \qquad (1)$$

$$\Phi_1(\mathbf{D_2}^{+}) = \Phi_2(\mathbf{D_3}^{++}) = \Phi_{total} \qquad \text{(reverse bias)} \qquad (2)$$

$$\Phi_1(\mathbf{D_2}^{++}) = \Phi_2(\mathbf{D_3}^{+}) = \Phi_{total} \qquad \text{(forward bias)} \qquad (3)$$

$\Phi_1(\mathbf{D_2}^{+})$ and $\Phi_2(\mathbf{D_3}^{++})$ defined as surface concentrations of diquat subunits of the specified oxidation state in formal 'monolayers' at the redox junction, $k_{(\mathbf{D_2} \rightarrow \mathbf{D3})}$ = interfacial, sur-

---

[9]) Except for the missing additional current due to $V_{CN}^{+} \rightarrow V_{CN}^{0}$ reduction.

[10]) From *Eqns. 1* and *2* (*cf. Chapt. 8*) and using the experimental value $i_l = 125 \pm 25 \cdot 10^{-6}$ A/cm^2, we find $\Phi^2 \cdot k_{(\mathbf{D_2} \rightarrow \mathbf{D3})} = 1.3 \cdot 10^{-9}$ mol/cm^2·s, *i.e.* a value 5 times smaller than reported for the bilayer-film-modified electrode poly[Os(bpy)$_2$(vpy)$_2$]$^{2+}$/poly[Ru(vbpy)$_3$]$^{2+}$ polarized in backward direction, inspite that the e.t. at the polymer/polymer interface in the diquat diode is by 180 mV less endergonic than in the Os/Ru diode [9e]. However, Φ's and k(self-exchange)'s for the two bilayers may differ substantially from the diquat diode.

face rate constant for reverse bias ($cm^2/mol \cdot s$), n = number of electrons, A = surface (cm^2), and F = *Faraday* constant. Assuming that the reverse bias (more negative potential at the electrode in contact with $\mathbf{D}_2$) is larger than $E°(\mathbf{D}_2^{++}/\mathbf{D}_2^{+}) - E°(\mathbf{D}_3^{++}/\mathbf{D}_3^{+})$, that the $\mathbf{D}_2^{+}/\mathbf{D}_2^{\circ}$ and $\mathbf{D}_3^{+}/\mathbf{D}_3^{\circ}$ couple do not interfere, and that $\Phi_1(\mathbf{D}_2^{+})$ and $\Phi_2(\mathbf{D}_3^{++})$ are in *Nernst*ian equilibrium with their electrode potential, the Φ's can then be described by *Eqn. 2*. For the sake of clarity, let's further simplify the problem. We assume that under large forward bias, *i.e.* the more negative potential being now applied to the electrode in contact with $\mathbf{D}_3$, e.t. in each polymer film is much faster than at the redox junction and thus, that no concentration gradient of redox sites develops within each film and that *Eqn. 3* holds. In this case – and assuming further activated-complex theory to hold – the current ratio under forward and

$$\frac{i_{l(f.b.)}}{i_{l(r.b.)}} = \frac{k_{(\mathbf{D_3} \rightarrow \mathbf{D_2})}}{k_{(\mathbf{D_2} \rightarrow \mathbf{D_3})}} = K_{f.b.} = \exp\left[\frac{n \cdot F}{R \cdot T}\,(E°(\mathbf{D}_2^{++}/\mathbf{D}_2^{+}) - E°(\mathbf{D}_3^{++}\text{–}\mathbf{D}_3^{+}))\right] \qquad (4)$$

reverse polarization can be described by *Eqn. 4*. For a vectorial electrochemical gradient of 220 mV, *Eqn. 4* yields ($i_{l(f.b.)}/i_{l(r.b.)} = K = 5.2 \cdot 10^3$. In reality, the current ratio is much smaller, because e.t. under forward bias is limited by the self-exchange rate [6] and/or by diffusional processes[11]) rather than by the exergonic e.t., as assumed in *Eqn. 4*. The result is still interesting as it describes the current ratio of the ideal redox-polymer bilayer-film-based diode[12]).

The most fundamental semiconductor devices together with their redox-polymer, bi- or multilayer-based analoga are shown in *Fig. 7*[13]). Some have been realized, others are hypothetical, either predicted earlier by *Murray* and *Wrighton* or presented here for the first time. A diode is expected to result, if two segregated polymer films, each exhibiting one redox level, are sandwiched between two conductors [13] [14]. $\Delta E°$ appears as the minimal voltage for current on-set in forward direction and governs the leakage current under reverse bias (*Fig. 7a*). A *Zener* diode is expected from a sandwiched bilayer of two redox polymer, one exhibiting two redox levels, the other polymer one redox level, located energetically in-between (*Fig. 7b*). $\Delta E_1°$ determines the current on-set voltage under forward bias, $\Delta E_2°$ the current break-through voltage under reverse bias[14]). More sophisticated functions can be achieved with sandwiched multilayers. A transistor is

---

[11]) Charge transport in the polymer is usually treated as a diffusional process [30].

[12]) If one takes a more realistic film model, *e.g.* the assembly electrode/$\mathbf{D}_2/\mathbf{D}_2/\mathbf{D}_3/\mathbf{D}_3$/electrode, with $\mathbf{D}_2$ and $\mathbf{D}_3$ corresponding to formal monolayers, and assuming self-exchange e.t. limitation by the $\mathbf{D}_2/\mathbf{D}_2$ and $\mathbf{D}_3/\mathbf{D}_3$ interface under forward bias, and *Eqn. 5* and *6* to hold, the *Marcus* cross-relation yields *Eqn. 7*:

$$k_{(\mathbf{D_2} \rightarrow \mathbf{D_2})} \approx k_{(\mathbf{D_3} \rightarrow \mathbf{D_3})} = k_{(\mathbf{D})} \qquad (5)$$

$$f_{(\mathbf{D_2} \rightarrow \mathbf{D_2})} \approx f_{(\mathbf{D_3} \rightarrow \mathbf{D_3})} = 1 \qquad (6)$$

$$i_{l(f.b.)}/i_{l(r.b.)} = k_{(\mathbf{D})}/k_{(\mathbf{D_2} \rightarrow \mathbf{D_3})} = K_{f.b.}^{1/2} \qquad (7)$$

[13]) The most simple arrangement, *i.e.* a single redox-polymer sandwiched between two conductors is not shown in *Fig. 7*. Such devices exhibit redox-state-dependent conductivity. For an electron-hopping mechanism, it reaches a maximum for a 1:1 mixed-valence state. As the [Red]/[Ox] ratio – and thus the current – can be controlled by a potential (*vs.* a reference electrode), such devices were compared with FET's (field-effect transistors) [31].

[14]) The open-face version of the *Zener* diode leads to charge-trapping, charge-untrapping phenomena.

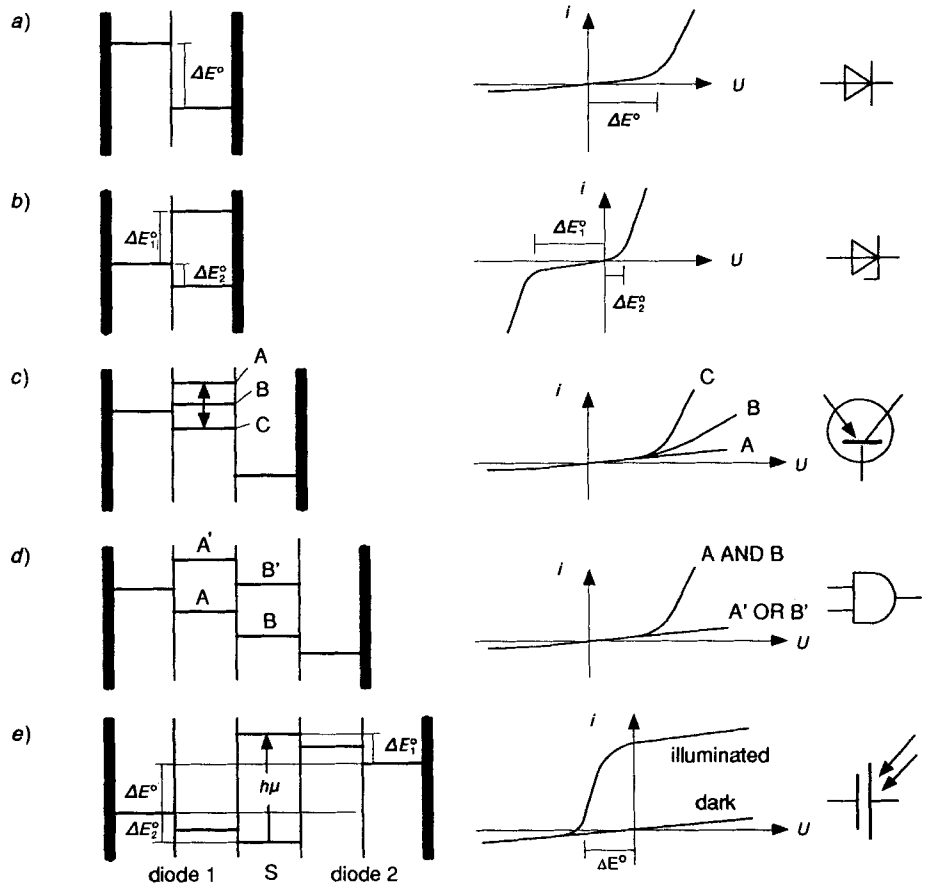

Fig. 7. *Electronic devices based on redox junctions. a*) Diode; ΔE° = current on-set potential for forward bias. *b*) *Zener* diode; ΔE_2° = current on-set voltage; ΔE_1° = current break-through voltage. *c*) Chemically biased transistor: collector and emitter with fixed redox potentials, base with a chemically tuned potential. *d*) Chemo-logical AND gate with two redox levels responding to two compounds a (A′→A) and b (B′→B). *e*) Solar cell consisting of a sensitizer film (S) flanked by two diodes, ΔE° = open-circuit voltage under illumination; $\Delta E_1^\circ + \Delta E_2^\circ$ = dissipated energy.

shown in *Fig. 7c*. It consists formally of a redox diode polarized in forward direction with an intermediary redox polymer with adjustable redox level. Depending on the relative height of this level, current flows through the forward-biased cascade. The middle redox level may be adjusted by specifically interfering molecular guests, and the current will be modulated by this interaction. Thus, the device acts as a chemical sensor with build-in amplifier[15]). *Fig. 7d* shows the principle of a chemo-logical gate with AND function.

[15]) There exist some similarities between this arrangement and CHEM-FET's, however, the device of *Fig. 7c* is not restricted to charged analytes [32].

Assuming that the two intermediary redox levels (A,A′ and B,B′) are controlled by the presence of two chemical compounds a and b indepedently, forward current will flow only, if level A AND B are available, *i.e.* if compound a AND b are present[16]). *Fig. 7e* represents a photovoltaic device based on a sequence of five redox polymers sandwiched between two conductors. The middle layer consists of a photosensitizer. It is flanked by two bilayers with electron donor (left), electron acceptor (right), and diode function (both). Upon irradiation, the photoexcited state is either oxidatively or reductively quenched by one of the two neighboring redox polymers, and irreversible charge separation is accomplished by the diodes. Depending on the charge capacity of the outermost redox-polymer films, energy storage could be achieved. The leakage (backward) current is related to ΔE_1° and ΔE_2°, the open-circuit voltage to ΔE°. We recently achieved large photocurrent with an open-face version of *Fig. 7d*, using our diquat diode (forward-biased) in combination with a polymeric [Ru(bpy)$_3$] film[17]). The results are reported in a separate publication [37]. Currently, sequential electropolymerization offers the easiest and most direct approach to complex film-type redox junctions. Molecular layers as obtainable by *Langmuir-Blodgett* or by self-assembling techniques would exhibit faster charge-propagation properties, but today, they are still prone to short circuits. Most of the redox-junction-based devices in *Fig. 7* are hypothetical, and the list is definitely not complete. Anyhow, chemists have just started to recognize the conceptual and synthetic challenge. A challenge, that is not just based on the competition between chemistry and solid-state physics. It is much more related to an exciting link between chip technology and molecular systems such as (bio)chemical signal transducers, amplifiers for chemical signals (catalysts), and energy converters.

We thank Dr. *Ch. Weymuth*, Prof. *H.-J. Hansen*, and Dr. *R. Fallahpour*, University of Zürich, for giving us access to their high-pressure equipment. We thank the *Swiss National Science Foundation* for financial support until autumn 1993 and hope that this research will be granted again in the near future.

Experimental Part

1. *General.* $NaHCO_3$ and Na_2CO_3 (*Siegfried PHHVI*), NaOH (*Siegfried, purum*), $NH_4(PF_6)$ (*Merck*), and $LiClO_4$ (*Biochemika micro Select*) were used as purchased. Et_2O (*Siegfried, PHHVI*) was distilled from NaH. All other reagents and solvents from *Fluka*: 4,4′-dimethyl-2,2′-bipyridine, *puriss.*; 1,2-dibromoethane and 1,3-dibromopropane, *purum*, distilled before use; chloroacetonitrile, *pract.*, distilled before use; pyrrole, *purum*, filtered through aluminium oxide before use; tetrabutylammonium bromide (Bu_4NBr), *purum*; tetrabutylammonium perchlorate ($Bu_4N(ClO_4)$), *purum*, recrystallized from AcOEt; tetrabutylammonium hexafluorophosphate ($Bu_4N(PF_6)$), *puriss.*; MeCN, *purum* (distilled over P_2O_5). Column chromatography (CC): silica gel (*J. T. Baker*; 30–60 μm). UV/VIS: *Hewlett-Packard-8451A* diode array spectrophotometer. IR: *Perkin-Elmer-782*. NMR: *Varian EM 360L* (^{1}H, 60 MHz) and *Bruker AC-300* (^{1}H, 300 MHz; ^{13}C, 75 MHz); Me_4Si ($CDCl_3$, (D_6)DMSO) or DSS (2,2-dimethyl-2-silapentane-5-sulfonate; D_2O) as internal reference, chemical shifts in ppm with $\delta(Me_4Si)$ or $\delta(DSS) = 0$; coupling constants J in Hz. MS: *Varian-MAT-CH-7A* mass spectrometer.

2. *Electrochemistry.* 2.1. *Devices.* An *Amel 553/Amel 568* was used as potentiostat/function generator. Voltammograms were recorded on a *Graphtec WX2400* X–Y recorder or with a digital data-acquisition system [38]. Cyclic voltammetry: all measurements were performed in *Metrohm* cells under Ar at 22 ± 2°. The working

---

[16]) *Aviram* has reported on molecular AND and OR gates [33].

[17]) Photocurrents at modified electrodes using bilayer assemblies [34] and molecular charge separators [35] or charge separation within soluble polymers [36] are of current interest.

electrode was a *Metrohm* (*6.0804.010*) glassy carbon electrode (active surface: 0.07 cm^2). After each measurement of a monomer or prior to a new electropolymerization, the surface was polished with Al_2O_3 (*Metrohm 6.2802.000*). The reference was a *Metrohm* (*6.0724.100*) KCl-sat. aq. calomel electrode (SCE), separated from the soln. by a salt bridge containing the same solvent and electrolyte as the soln. The counter electrode was a Pt-wire. Rotating-disc voltammetry: A rotating glassy carbon disc ($A = 0.2$ cm^2) driven by a *Metrohm-628-10* unit and fitted to a *Metrohm* cell was used.

2.2. *Electropolymerization.* All electropolymerizations were done at r.t. under strict exclusion of O_2. Monomers **4** and **5** (0.5 to $2 \cdot 10^3$ M) were cathodically electropolymerized on glassy carbon electrodes from solns. of 0.1M $Bu_4N(ClO_4)$/MeCN or 0.1M $Bu_4N(PF_6)$/MeCN (Ar bubbling). The electrode potential was either continuously scanned for 10–100 min at 0.1 V/s between 0 and −1 to −1.2 V *vs.* SCE, or it was hold for 10–100 min at −1 to −1.2 V. Scanning to or holding the potential at −0.5 to −0.7, *i.e.* between E_1° and E_2° resulted in much slower electropolymerization. Addition of H_2O (1–10%) did increase the rate of electropolymerization, and **5** was even electropolymerized from 0.1M $LiClO_4/H_2O$ (possibly from an adsorbed state) using a continuous scan from 0 to −1.0 or to −1.3 V, *i.e.* with or without involvement of the second redox couple. The PF_6 salts **6b** and **7b** ($0.5–0.7 \cdot 10^{-3}$ M) were oxidatively electropolymerized on glassy carbon electrodes from 0.1M $Bu_4N(ClO_4)$/MeCN (Ar bubbling). Such solutions – even kept in the dark and protected from O_2 – exhibited some aging, *i.e.* polymer formation from monomer solutions older than 2 h became difficult. Either a continuous potential scan (0.1 V/s) between 0 and +1.7 V was applied for 1–10 min, or a fixed potential of 1.3–1.4 V (located in the foot of the pyrrolyl oxidation) was applied for 1–10 min. The $\mathbf{D_2}$- and $\mathbf{D_3}$-redox-polymer monolayer-modified electrodes were prepared by copolymerization of pyrrole ($c = 0.15 \cdot 10^{-3}$ M) and **6b** ($c = 1.4 \cdot 10^{-3}$ M) or pyrrole ($c = 0.15 \cdot 10^{-3}$ M) and **7b** ($c = 1.4 \cdot 10^{-3}$ M) from 0.2M $Bu_4N(ClO_4)$/MeCN (Ar bubbling) using an electrode potential of +1.34 V for 60 and 75 s, resp. The ($\mathbf{D_2} + \mathbf{D_3}$)-modified electrodes were prepared by copolymerization of pyrrole ($c = 0.15 \cdot 10^{-3}$ M), **6b** ($c = 0.7 \cdot 10^{-3}$ M), and **7b** ($c = 0.7 \cdot 10^{-3}$ M) from 0.2M $Bu_4N(ClO_4)$/MeCN using an electrode potential of +1.34 V for 75 s (Ar bubbling). After polymerization, the modified electrodes were equilibrated for some s in the electrochemical cell at 0 V before they got into contact with air, to have all bipyridinium centers in their dicationic redox state, which is unreactive toward O_2. They were then rinsed with the same solvent as for electropolymerization and further used or air-dried and stored in the dark. Bilayer-polymer-modified electrodes were prepared by the sequential application of the above procedure with different monomer solutions on the same electrode.

2.3. *Electrochemistry of the Modified Electrodes.* All measurements on mono- and bilayer redox-polymer-modified electrodes were done in 0.1 or 0.2M $Bu_4N(ClO_4)$/MeCN (Ar bubbling). E° Values were determined from the peak potentials according to $E^\circ = (E_p(\text{cath.}) + E_p(\text{anod.}))/2$, surface concentrations (Γ's [mol/cm^2]) of bipyridinium subunits coulometrically by the CACYVO-implemented integration routine on the faradaic currents of the bipyridinium waves, obtained from slow-scan cyclic voltammograms [38]. The ratio of polymer-incorporated pyrrole/**6b** or pyrrole/**7b** was determined on the polypyrrole oxidation wave in $\mathbf{D_2}$ or $\mathbf{D_3}$ as compared to that of poly-**6b** and poly-**7b**, resp. An estimate of the polymer-film thickness was obtained from Γ's of **6b** (or **7b**) subunits and of unsubstituted pyrrole subunits, and assuming a molar volume for **6b**, V(**6b**) = 240 cm^3/mol (from model considerations) and for unsubstituted pyrrole subunits, V(pyr) = 72 cm^3/mol using *Eqn. 8* [26]. With $\Gamma_{pyr}/\Gamma_{\mathbf{6b}} = 2$, *Eqn. 8* reduces to *Eqn. 9*.

$$d = 72\,\Gamma_{pyr} + 240\,\Gamma_{\mathbf{6b}} \quad (8)$$

$$d = 384\,\Gamma_{\mathbf{6b}} \quad (9)$$

V_{CN}^{++} Reduction at the mono- or bilayer-modified rotating-disc electrode was done with $1 \cdot 10^{-3} < [\mathbf{8}] < 8 \cdot 10^{-3}$ M in 0.2M $Bu_4N(ClO_4)$/MeCN + pyridin ($50 \cdot 10^{-3}$ M) ($A = 0.2$ cm^2, $v = 780$ rpm, $\nu = 5$ mV/s). The pyridin was added as a base to prevent protonation of redox-confined, reduced bipyridinium units by **8**.

3. *Syntheses.* 3.1. *4-Methyl-4′-vinyl-2,2′-biypridine* (**2**). Following [20], 4-(2-methoxyethyl)-4′-methyl-2,2′-bipyridine (**1**; also prepared according to [20]; 10.0 g, 44 mmol) yielded 9.3 g of crude **2** as a yellow powder. It was purified by CC (137 g of silica gel, 4.5 × 35 cm, Et_2O/0.8% aq. NH_3 soln.), dried, and, after solvent evaporation, crystallized from a minimum amount of Et_2O. Drying *in vacuo* (r.t., 24 h) gave **2** (7.0 g, 81%). Colorless crystals. M.p. 65.5–66.5°. UV/VIS (MeOH, $c = 4.5 \cdot 10^{-5}$ M): 210 (4.41), 240 (4.48), 282 (4.04). IR (KBr): a.o. 3060*w*, 2930*w*, 1590*s*, 1550*m*, 1460*m*, 1360*m*, 990*m*, 930*m*, 830*m*, 810*m*. ^{1}H-NMR (300 MHz, $CDCl_3$): 2.43 (*s*, Me–C(4)); 5.51 (*dd*, $J = 2$, 10.9, 1 H, CH_2=CH, *cis*); 6.09 (*dd*, $J = 2$, 17.6, 1 H, CH_2=CH, *trans*); 6.76 (*dd*, $J = 10.9$, 17.6, CH_2=C*H*); 7.13 (*dd*, $J = 2$, 4.4, H–C(5)); 7.29 (*dd*, $J = 2$, 5.1, H–C(5′)); 8.24 (*d*, $J = 2$, H–C(3)); 8.40 (*d*, $J = 2$, H–C(3′)); 8.54 (*d*, $J = 4.8$, H–C(6)); 8.61 (*d*, $J = 5.1$, H–C(6′)). ^{13}C-NMR (300 MHz, $CDCl_3$): 21.2 (Me–C(4)); 118.5 (CH_2=CH); 118.8, 120.6 (C(5), C(5′)); 122.0, 124.8 (C(3), C(3′)); 135.0 (CH_2=*C*H); 145.80, 148.2 (C(4), C(4′)); 149.0, 149.4 (C(6), C(6′)); 155.7, 156.7 (C(2), C(2′)). MS: 196 (100, M^+), 181 (7, $[M - Me]^+$), 170 (70,

$[M - C_2H_2]^+$), 142 (7), 104 (5, $C_5H_3NCHCH_2^+$), 92 (8, $C_5H_3NCH_3^+$), 77 (6), 65 (6). Anal. calc. for $C_{13}H_{12}N_2$ (196.25): C 79.56, H 6.16, N 14.27; found: C 79.61, H 5.85, N 14.40.

3.2. *4-Methyl-4'-[2-(1H-pyrrol-1-yl)ethyl]-2,2'-bipyridine* (**3**). In pieces, Na (100 mg) was added to a rapidly stirred soln. of 1*H*-pyrrole (4.0 g, 60 mmol) and **2** (1.0 g, 5.1 mmol) [21]. The mixture was heated to reflux for *ca.* 4 h and then cooled to r.t. After addition of abs. EtOH (1 ml), the soln. was poured into ice-water (40 ml) and extracted with Et_2O (3 × 40 ml), the extract dried and evaporated, and the residue dried *in vacuo* (r.t., 24 h): 1.2 g (90%) of **3** as a slightly colored solid. The product was used without further purification in the following reaction. An anal. sample was obtained by recrystallization from Et_2O. M.p. 92–93°. UV/VIS (MeOH, $c = 3.5 \cdot 10^{-5}$ M): 208 (4.51), 236 (4.11), 284 (4.16). IR (KBr): 3100*w*, 2910*w*, 1600*s*, 1550*w*, 1500*w*, 1450*m*, 820*m*, 750*s*. ^{1}H-NMR (300 MHz, $CDCl_3$): 2.45 (*s*, Me–C(4)); 3.14 (*t*, $J = 7.4$, CH_2CH_2–C(4')); 4.19 (*t*, $J = 7.4$, CH_2CH_2–C(4')); 6.13 (*t*, $J = 2.1$, H–C(3''), H–C(4'')); 6.61 (*t*, $J = 2.1$, H–C(2''), H–C(5'') (pyrr)); 6.94 (*dd*, $J = 5.0, 1.7$, H–C(5')); 7.16 (*d*, $J = 4.1$, H–C(5)); 8.23 (*d*, $J = 2$, H–C(3')); 8.25 (*d*, $J = 2$, H–C(3)); 8.55 (*d*, $J = 4.9$, H–C(6), H–C(6')). ^{13}C-NMR (300 MHz, $CDCl_3$): 21.2 (Me–C(4)); 38.0 (CH_2CH_2–C(4')); 50.0 (CH_2CH_2–C(4')); 108.4 (C(3''), C(4'') (pyrr)); 120.5 (C(2''), C(5'') (pyrr)); 121.2, 122.1 (C(5), C(5')); 124.1, 124.8 (C(3), C(3')); 148.2, 148.3 (C(4), C(4')); 149.0, 149.3 (C(6), C(6')); 155.5, 156.5 (C(2), C(2')). MS: 263 (60, M^+), 262 (100, $[M - 1]^+$), 235 (20, $[M - CH_2CH_2]^+$), 197 (10, $[M - \text{pyrr}]^+$), 184 (45, $[M - C_4H_4NCH]^+$), 171 (15), 92 (5), 80 (45). Anal. calc. for $C_{17}H_{17}N_3$ (263.34): C 77.54, H 6.51, N 15.96; found: C 77.06, H 6.42, N 15.84.

3.3. *N,N'-Ethylene-4-methyl-4'-vinyl-2,2'-bipyridinium Dibromide* (**4**). Following [9c], **2** (392 mg, 2.0 mmol) in 1,2-dibromoethane (5 ml) was stirred under N_2 at 100° for 25 h. The resulting precipitate was filtered and washed with Et_2O and hexane. Drying *in vacuo* (r.t., 24 h) gave 0.80 g (> 100%; not corrected for some H_2O content) of **4**. Light yellow, hygroscopic powder. UV/VIS (MeOH, $c = 5.5 \cdot 10^{-5}$ M): 208 (4.34), 308 (4.04). IR (KBr): 3000*s*, 1620*s*, 1585*m*, 1510*m*, 1455*m*, 1290*m*, 1240*m*, 1175*m*, 840*w*. ^{1}H-NMR (60 MHz, D_2O): 2.90 (*s*, Me–C(4)); 5.30 (*m*, NCH_2CH_2N); 6.10–7.30 (*ABX*, CH_2=C–C(4')); 8.20–8.60 (*m*, H–C(5), H–C(5')); 8.90–9.30 (*m*, H–C(3), H–C(3'), H–C(6), H–C(6')). The broad peaks indicate partial reduction of **4** to the radical cation.

3.4. *4-Methyl-N,N'-(trimethylene)-4'-vinyl-2,2'-bipyridinium Dibromide* (**5**). As described for **4**, using 1,3-dibromopropane instead of 1,2-dibromoethane and 0.39 g (2 mmol) of **2**: 0.9 g (> 100%; not corrected for residual H_2O) of **5**. Light yellow, hygroscopic powder. UV/VIS (MeOH, $c = 6.5 \cdot 10^{-5}$ M): 214 (4.36), 288 (4.11). IR (KBr): 3000*s*, 1620*s*, 1580*m*, 1510*m*, 1450*m*, 1360*w*, 850*w*. ^{1}H-NMR (60 MHz, D_2O): 2.80 (*s*, Me–C(4)) overlapped by 2.50–3.20 (*m*, $NCH_2CH_2CH_2N$); 4.20–5.30 (*m*, $NCH_2CH_2CH_2N$); 6.15 (*d*, $J = 10$, 1 H, CH_2=CH, *cis*); 6.75 (*d*, $J = 17$, 1 H, CH_2=CH, *trans*); 7.20 (*dd*, $J = 10, 17$, CH_2=CH); 8.10–8.70 (*m*, H–C(3), H–C(3'), H–C(5), H–C(5')); 8.90–9.25 (*m*, H–C(6), H–C(6')).

3.5. *N,N'-Ethylene-4-methyl-4'-[2-(1H-pyrrol-1-yl)ethyl]-2,2'-bipyridinium Bis(hexafluorophosphate)* (**6b**).

3.5.1. A soln. of **3** (1.15 g, 4.4 mmol) in 1,2-dibromoethane (10 ml) was heated at 100° for 24 h. The resulting precipitate was filtered and washed with Et_2O. Drying *in vacuo* (r.t., 24 h) gave 1.64 g (81%) of dibromide **6a**. It was dissolved in a minimum amount of H_2O and dropped into a stirred soln. of $NH_4(PF_6)$ (2 g) in H_2O (15 ml). The precipitate was filtered, washed with H_2O, and dried *in vacuo* (r.t., 24 h): **6b** (quant.) as a charge-transfer complex with 1 equiv. of NH_3.

3.5.2. A soln. of **3** (1 g, 3.8 mmol) in 1,2-dibromoethane (4 ml) and MeCN (8 ml) was kept for 48 h at 50° and 5.5 kbar. The solvent was evaporated, the precipitate dissolved in H_2O, and the anion exchanged as in 3.5.1: 0.7 g (32%) of **6b**. UV/VIS (MeOH, $c = 5.5 \cdot 10^{-5}$ M): 216 (4.04), 310 (3.85). IR (KBr): 3100*w*, 1630*m*, 1470*m*, 850*s*, 570*s*. ^{1}H-NMR (300 MHz, (D_6)DMSO): 2.77 (*s*, Me–C(4)); 3.47 (*t*, $J = 6.7$, CH_2CH_2–C(4')); 4.40 (*t*, $J = 6.8$, CH_2CH_2–C(4')); 5.13 (*s*, NCH_2CH_2N); 5.99 (*t*, $J = 2.0$, H–C(3''), H–C(4'') (pyrr)); 6.77 (*t*, $J = 2.0$, H–C(2''), H–C(5'') (pyrr)); 8.12 (*d*, $J = 6.2$, H–C(5')); 8.26 (*d*, $J = 5.8$, H–C(5)); 8.82 (*d*, $J = 3.0$, H–C((3')); 8.84 (*d*, $J = 3.0$, H–C(3)); 9.14 (2*d*, H–C(6), H–C(6')). ^{13}C-NMR (300 MHz, (D_6)DMSO): 22.0 (Me–C(4)); 37.4 (CH_2CH_2–C(4')); 47.7 (CH_2CH_2–C(4')); 51.8, 51.9 (NCH_2CH_2N); 108.3 (C(3''), C(4'') (pyrr)); 120.9 (C(2''), C(5'') (pyrr)); 127.7, 128.0 (C(5), C(5')); 129.7, 130.2 (C(3), C(3')); 139.3, 139.5 (C(2), C(2')); 146.3, 146.4 (C(4), C(4')); 161.1, 161.2 (C(6), C(6')). Anal. calc. for $C_{19}H_{21}F_{12}N_2P_2$ (567.29): C 40.23, H 3.73, N 4.94; calc. for $C_{19}H_{21}F_{12}N_2P_2 \cdot NH_3$ (584.33): C 39.05, H 4.15, N 7.19; found: C 39.18, H 3.58, N 7.34.

3.6. *4-Methyl-4'-[2-(1H-pyrrol-1-yl)ethyl]-N,N'-(trimethylene)-2,2'-bipyridinium Bis(hexafluorophosphate)* (**7b**). As described for **6a** (see *3.5*), using 1,3-dibromopropane instead of 1,2-dibromoethane and **3** (0.80 g, 3.0 mmol): 1.45 g (100%) of dibromide **7a**. Anion exchange and drying *in vacuo* (r.t., 24 h) gave **7b** (quant.) as a solid charge-transfer complex with 1 equiv. of NH_3. UV/VIS (MeOH, $c = 2.7 \cdot 10^{-5}$ M): 208 (4.55), 288 (4.14). IR (KBr): 3000*s* (br.), 1630*s*, 1580*m*, 1510*m*, 1450*s*, 1360*w* (br.), 1310*m*, 1280*m*, 1260*w*, 1210*w*, 1175*m*, 1160*m*, 1145*w*, 1125*w*, 1090*m*, 1065*w*, 1035*w*, 830*m* (br.), 750*m*, 630*w*, 600*w*, 565*w*, 515*m*, 470*w*. ^{1}H-NMR (300 MHz, (D_6)DMSO): 2.74 (*m*, Me–C(4), NCH_2CH_2N); 3.43 (*t*, CH_2CH_2–C(4')); 4.35 (*m*, CH_2CH_2–C(4'), NCH_2CH_2N); 4.90 (*d*, NCH_2CH_2N); 6.01 (*t*, $J = 2.0$, H–C(3''), H–C(4'') (pyrr)); 6.77 (*t*, $J = 2.0$, H–C(2''), H–C(5'') (pyrr)); 8.12 (*d*,

H–C(3')); 8.16 (*dd*, J = 6.2, H–C(5')); 8.21 (*d*, H–C(3)); 8.30 (*dd*, J = 6.1, H–C(5)); 9.17 (*m*, H–C(6), H–C(6')). ^{13}C-NMR (300 MHz, (D$_6$)DMSO): 21.8 (*Me*–C(4)); 30.2 (NCH$_2$*C*H$_2$CH$_2$N); 37.4 (CH$_2$*C*H$_2$–C(4')); 48.0 (*C*H$_2$CH$_2$–C(4')); 54.8, 55.0 (N*C*H$_2$CH$_2$*C*H$_2$N); 108.3 (C(3''), C(4'') (pyrr)); 121.0 (C(2''), C(5'') (pyrr)); 130.3, 130.7 (C(5), C(5')); 131.7, 132.0 (C(3), C(3')); 143.2, 143.3 (C(4), C(4')); 146.8, 147.0 (C(2), C(2')); 160.7, 160.8 (C(6), C(6')). Anal. calc. for $C_{20}H_{23}F_{12}N_2P_2$ (581.32): C 41.32, H 3.99, N 4.82; calc. for $C_{20}H_{23}F_{12}N_2P_2 \cdot NH_3$ (598.36): C 40.14, H 4.38, N 7.02; found: C 40.07, H 3.55, N 7.20.

3.7. *N-(Cyanomethyl)-N'-methyl-4,4'-bipyridinium Bis(hexafluorophosphate)* (**8**). A soln. of *N*-methyl-4,4'-bipyridinium diodide (0.45 g, 1.5 mmol; prepared according to [9c]) and chloroacetonitrile (0.8 g, 10.6 mmol) in DMF was stirred for 72 h at 50° under Ar. The resulting precipitate was isolated, dissolved in a minimum amount of H_2O, and dropped into a soln. of $NH_4(PF_6)$ (1.6 g, 10 mmol) in H_2O (45 ml). The resulting white precipitate was isolated and dried *in vacuo* (r.t., 5 h): 0.32 g (43%) of **8**. UV/VIS (MeCN, $c = 1.7 \cdot 10^{-5}$ M): 198 (4.75), 262 (4.63), 536 (3.46). IR (KBr): 3180*m*, 3150*m*, 3030*w*, 2990*w*, 2350*w*, 1950 (br.), 1650*s*, 1570*m*, 1510*m*, 1460*m*, 1430*w*, 1360*w*, 1350*m*, 1280*w*, 1230*w*, 1195*m*, 830*s*, 740*w*, 720*w*, 560*s*, 500*w*, 450*w*. ^{1}H-NMR (300 MHz, (D$_6$)DMSO): 4.43 (*s*, MeN); 6.02 (*s*, CH$_2$N); 8.73 (*d*, J = 6.1, H–C(3), H–C(5)); 8.83 (*d*, J = 6.3, H–C(3'), H–C(5')); 9.27 (*d*, J = 6.2, H–C(2), H–C(6)); 9.46 (*d*, J = 6.3, H–C(2'), H–C(6')). ^{13}C-NMR (300 MHz, (D$_6$)DMSO): 48.0 (MeN); 48.3 (CH$_2$N); 114.3 (CN); 126.5, 127.2 (C(3), C(5), C(3'), C(5')); 146.7, 146.9 (C(2), C(6), C(2'), C(6')); 148.1 (C(4)); 150.7 (C(4')).

REFERENCES

[1] a) C. Kittel, 'Introduction to Solid State Physics', 6th edn., J. Wiley, New York, 1986; b) L. Stryer, 'Biochemistry', Ed. W. H. Freeman, New York, 1988; c) P. Mathis, *Pure Appl. Chem.* **1990,** *62,* 1521; d) V. Balzani, F. Scandola, 'Supramolecular Photochemistry', Ellis Horwood, New York, 1991; e) T.J. Meyer, *Acc. Chem. Res.* **1989,** *22,* 163.

[2] R.M. Baum, *Chem. Eng. News* **1993,** *71,* 20.

[3] 'Molecular Electronic Devices', Ed. F.L. Carter, Marcel Dekker, New York, 1982, Vol. I; *ibid.*, 1987, Vol. II; R.M. Metzger, C.A. Panetta, *New J. Chem.* **1991,** *15,* 209; D. Bradley, *Science* **1993,** *259,* 890; W. Göpel, *Sensors Actuators B* **1991,** *4,* 7.

[4] A. Aviram, M.A. Ratner, *Chem. Phys. Lett.* **1974,** *29,* 277.

[5] a) C. Joachim, *New J. Chem.* **1991,** *15,* 223; b) A.S. Martin, J.R. Sambles, G.J. Ashwell, *Phys. Rev. Lett.* **1993,** *70,* 218; c) G.J. Ashwell, J.R. Sambles, A.S. Martin, W.G. Parker, M. Szablewski, *J. Chem. Soc., Chem. Commun.* **1990,** 1374.

[6] a) R.A. Marcus, *Discuss. Faraday Soc.* **1960,** *29,* 21; b) R.A. Marcus, *J. Phys. Chem.* **1965,** *43,* 679.

[7] a) B. Steiger, L. Walder, *Helv. Chim. Acta* **1992,** *75,* 90; b) D.K. Smith, G.A. Lane, M.S. Wrighton, *J. Am. Chem. Soc.* **1986,** *108,* 3522; c) D.K. Smith, L.M. Tender, G.A. Lane, M.S. Wrighton, *ibid.* **1989,** *111,* 1099; d) W.J. Vining, N.A. Surridge, T.J. Meyer, *J. Phys. Chem.* **1986,** *90,* 2281.

[8] J. Heinze, *Topics Curr. Chem.* **1990,** *152,* 1; A. Merz, *ibid.* **1990,** *152,* 49; R.W. Murray, in 'Electroanalytical Chemistry', Ed. A.J. Bard, Marcel Dekker, New York, 1984, Vol. 13, p. 191.

[9] a) H.D. Abruña, P. Denisevich, M. Umaña, T.J. Meyer, R.W. Murray, *J. Am. Chem. Soc.* **1981,** *103,* 1; b) P. Denisevich, K.W. Willman, R.W. Murray, *ibid.* **1981,** *103,* 4727; c) K.W. Willman, R.W. Murray, *J. Electroanal. Chem.* **1982,** *133,* 211; d) P.G. Pickup, C.R. Leidner, P. Denisevich, R.W. Murray, *ibid.* **1984,** *164,* 39; e) C.R. Leidner, R.W. Murray, *J. Am. Chem. Soc.* **1985,** *107,* 551.

[10] A.R. Hillman, E.F. Mallen, *J. Electroanal. Chem.* **1990,** *281,* 109; K. Murao, K. Suzuki, *Solid State Commun.* **1987,** *62,* 483; R.N. O'Brien, K.S.V. Santhanam, *Mater. Chem. Phys.* **1987,** *18,* 19.

[11] M. Aizawa, H. Shinohara, T. Yamada, H. Shirakawa, *Synth. Met.* **1987,** *18,* 711; W. Torres, M.A. Fox, *Chem. Mater.* **1990,** *2,* 306.

[12] C.E.D. Chidsey, R.W. Murray, *Science* **1986,** *231,* 25; M.S. Wrighton, *ibid.* **1986,** *231,* 33; R.W. Murray, A.G. Ewing, R.A. Durst, *Anal. Chem.* **1987,** *59,* 379A; M.J. Natan, M.S. Wrighton, *Progr. Inorg. Chem.* **1989,** *37,* 391.

[13] J.C. Jernigan, R.W. Murray, *J. Am. Chem. Soc.* **1990,** *112,* 1034.

[14] G.P. Kittelsen, H.S. White, M.S. Wrighton, *J. Am. Chem. Soc.* **1985,** *107,* 7373; G.P. Kittelsen, M.S. Wrighton, *J. Mol. Electron.* **1985,** *2,* 23.

[15] D.R. Prasad, G. Ferraudi, *Inorg. Chem.* **1983,** *22,* 1672; b) F. Vögtle, D. Brombach, *Chem. Ber.* **1975,** *108,* 1682.

[16] D. H. Evans, K. M. O'Connell, in 'Electroanalytical Chemistry', Ed. A. J. Bard, Marcel Dekker, New York, 1986, Vol. 14, p. 113; D. H. Evans, *Chem. Rev.* **1990,** *90,* 739.
[17] a) I. Willner, A. Ayalon, M. Rabinovitz, *New J. Chem.* **1990,** *14,* 685; b) A. Launikonis, J. W. Loder, A. W.-H. Mau, W. H. F. Sasse, D. Wells, *Isr. J. Chem.* **1982,** *22,* 158; c) I. C. Calder, McL. Spotswood, C. I. Tanzer, *Aust. J. Chem.* **1967,** *20,* 1195; d) McL. Spotswood, C. I. Tanzer, *ibid.* **1967,** *20,* 1213; e) McL. Spotswood, C. I. Tanzer, *ibid.* **1967,** *20,* 1227.
[18] D. A. Kleier, G. H. Weeks, *J. Mol. Struct.* **1986,** *148,* 25; H.-J. Hofmann, R. Cimiraglia, I. Tomasi, *ibid.* **1986,** *139,* 213.
[19] a) S. Cosnier, A. Deronzier, J.-C. Moutet, *J. Electroanal. Chem.* **1985,** *193,* 193; b) S. Cosnier, A. Deronzier, J.-C. Moutet, *J. Mol. Catal.* **1988,** *45,* 381; c) S. Cosnier, H. Gunther, *J. Electroanal. Chem.* **1991,** *315,* 307; d) S. Cosnier, A. Deronzier, J.-C. Moutet, *New J. Chem.* **1990,** *14,* 831; e) S. Cosnier, A. Deronzier, J.-F. Roland, *J. Electroanal. Chem.* **1990,** *185,* 133.
[20] H. D. Abruña, A. I. Breikss, D. B. Collum, *Inorg. Chem.* **1985,** *24,* 987.
[21] H. E. Reich, R. Levine, *J. Am. Chem. Soc.* **1955,** *77,* 4913.
[22] C. J. Baldy, D. L. Morrison, C. M. Elliott, *Langmuir* **1991,** *7,* 2376.
[23] A. Deronzier, J.-C. Moutet, *Acc. Chem. Res.* **1989,** *22,* 249.
[24] P. Bäuerle, K.-U. Gaudl, *Adv. Mat.* **1990,** *2,* 185; P. Janda, J. Weber, L. Kavan, *J. Electroanal. Chem.* **1984,** *180,* 109; K. Shigehara, E. Tsuchida, F. C. Anson, *ibid.* **1984,** *175,* 291; G. Bidan, A. Deronzier, J.-C. Moutet, *J. Chem. Soc., Chem. Commun.* **1984,** 1185; L. Coche, A. Deronzier, J.-C. Moutet, *J. Electroanal. Chem.* **1986,** *198,* 187.
[25] A. Haimerl, A. Merz, *Angew. Chem.* **1986,** *98,* 179.
[26] J. Ochmanska, P. G. Pickup, *J. Electroanal. Chem.* **1989,** *271,* 83.
[27] T. Ikeda, C. R. Leidner, R. W. Murray, *J. Electroanal.Chem.* **1982,** *138,* 343.
[28] C. R. Leidner, R. W. Murray, *J. Am. Chem. Soc.* **1984,** *106,* 1606.
[29] P. G. Pickup, R. W. Murray, *J. Electrochem. Soc.* **1984,** *131,* 832.
[30] E. Laviron, *J. Electroanal. Chem.* **1980,** *112,* 1; C. P. Andrieux, J.-M. Savéant, *ibid.* **1980,** *111,* 377; D. N. Blauch, J.-M. Savéant, *J. Am. Chem. Soc.* **1992,** *114,* 3323.
[31] P. G. Pickup, W. Kutner, C. R. Leidner, R. W. Murray, *J. Am. Chem. Soc.* **1984,** *106,* 1991; J. C. Jernigan, C. E. D. Chidsey, R. W. Murray, *ibid.* **1985,** *107,* 2824; C.-H. Shu, M. S. Wrighton, *J. Phys. Chem.* **1988,** *92,* 5221.
[32] J. N. Zemel, *Anal. Chem.* **1975,** *47,* 255A.
[33] A. Aviram, *J. Am. Chem. Soc.* **1988,** *110,* 5687.
[34] Y. Morishima, Y. Fukushima, S. Nozakura, *J. Chem. Soc., Chem. Commun.* **1985,** 912.
[35] A. Deronzier, M. Essakalli, *J. Chem. Soc., Chem. Commun.* **1990,** 242.
[36] S. M. Baxter, W. E. Jones, E. Danielson, L. Worl, G. Strouse, J. Younathan, T. J. Meyer, *Coord. Chem. Rev.* **1991,** *111,* 47.
[37] J. Marfurt, W. Zhao, L. Walder, *J. Chem. Soc., Chem. Commun.*, in press.
[38] B. Flückiger, L. Walder, unpublished results.